Nuclear Engineering and Technology 50 (2018) 1131–1137

Contents lists available at ScienceDirect

Nuclear Engineering and Technology

journal homepage: www.elsevier.com/locate/net

Original Article

Effect of serrated grain boundary on stress corrosion cracking of Alloy 600

H.P. Kim*, M.J. Choi, S.W. Kim, D.J. Kim, Y.S. Lim, S.S. Hwang

Nuclear Materials Research Division, Korea Atomic Energy Research Institute, 989-111 Daedeok-daero, Yuseong-gu, Daejeon, 305-353, Republic of Korea

ARTICLE INFO

Article history:
Received 25 March 2018
Received in revised form
15 May 2018
Accepted 29 May 2018
Available online 1 June 2018

Keywords:
Alloy 600
Stress corrosion cracking
Serrated grain boundary
Tensile stress
NaOH

ABSTRACT

The effect of a serrated grain boundary on stress corrosion cracking (SCC) of Alloy 600 was investigated in terms of improvement of SCC resistance. Serrated grain boundaries and straight grain boundaries were obtained by controlled heat treatment. SCC cracks preferentially initiated and grew at grain boundaries normal to the tensile loading axis. Resolved tensile stress normal to the grain boundary was lower in serrated grain boundaries compared to straight grain boundaries. The specimen with serrated grain boundaries showed higher SCC resistance than that with straight grain boundaries due to a lower resolved tensile stress normal to the grain boundary.

1. Introduction

Stress corrosion cracking (SCC) of Alloy 600 is important issue in the nuclear power industry. Steam generator tube rupture [1], early replacement of the steam generator [2], cracks in the nozzle and penetration [3] due to SCC surprised the nuclear industry and gave rise to safety concerns regarding nuclear power plants.

SCC of Alloy 600 propagates mostly in intergranular mode, that is, along the grain boundary [4–8] but rarely in transgranular mode in a lead contaminated environment [9–11]. Accordingly, a great deal of research has been performed to understand the features of grain boundaries [12–16] and grain boundary modification [17–21] to mitigate SCC. The most classical approach is thermal treatment of Alloy 600. Mill annealed Alloy 600 was used in the steam generators of nuclear power plants in the early 1970s, and it experienced stress corrosion cracking (SCC) in both the primary coolant system and the secondary coolant system [21]. Thermally treated Alloy 600 was used in the late 1970s instead of mill annealed Alloy 600 on the basis of its resistance to SCC [22]. At the same time, impurities such as S and P were carefully controlled to retard segregation at grain boundaries [23,24]. This approach of thermal treatment in combination with impurities control has been partially successful in reducing SCC in nuclear power plants but SCC of thermally treated Alloy 600 remains an issue in the nuclear power industry. Another approach is to increase the bulk chromium content in nickel base alloy from about 15% of Alloy 600 to 30% of Alloy 690 [25]. Thermally treated Alloy 690 has been used as a steam tubing material in replaced steam generators and new nuclear power plants since 1989. The thermally treated Alloy 690 is almost immune to SCC in the primary coolant system, but is more susceptible to SCC in highly caustic solutions with lead contaminants compared to Alloy 600 [9,26,27]. Another approach is grain boundary energy reduction. For this strategy, the concept of “grain boundary design and control” was introduced with the purpose of improving various properties of polycrystalline materials by enhancing the frequency of low-energy boundaries in the grain boundary character distribution [17–20]. Enhancing the fraction of low energy fracture resistant boundaries is essential to achieve SCC resistance by grain boundary design a control. In general, low angle boundaries and symmetrical boundaries (twins) are particularly strong, and high angle boundaries are less strong. Grain boundary modification by the formation of a serrated grain boundary was proposed to improve creep resistance [28–30]. Nickel base alloys with a serrated grain boundary showed higher creep resistance, likely due to inhibition of grain boundary sliding. The serrated grain boundary can also be applied to improve SCC resistance. Several mechanistic studies on the formation of a serrated grain boundary have been conducted [31–33]. But there has been little work on the

* Corresponding author.
E-mail address: hpkim@kaeri.re.kr (H.P. Kim).

https://doi.org/10.1016/j.net.2018.05.009

effect of the serrated grain boundary resistance to SCC of Alloy 600.

In this work, the effect of a serrated grain boundary on SCC was studied to determine the viability of improving SCC resistance of nickel base alloys with a serrated grain boundary.

2. Experimental procedure

The chemical composition of Alloy 600 used in this work is shown in Table 1. Serrated boundary specimens were solution treated at 1100 °C for 20min and then slowly cooled to 750 °C at a cooling rate of 0.3 °C/min and then water quenched to room temperature for the SA1+SERR specimen or additionally heat treated at 710 °C for 15 hrs for the SA1+SERR + TT specimen. The straight grain boundary specimens were solution treated at 1100 °C for 30min and then water quenched to room temperature in the case of the SA2 specimen, followed by thermal treatment at 710 °C for 15 hrs for the SA2+TT specimen. By controlling the solution heat treatment time and the cooling rate, the grain size of a serrated boundary and a straight boundary was almost the same. However, the density and size of intergranular carbide showed a slight difference between the serrated grain boundary specimen (SA1+SERR + TT) and the straight grain boundary specimen (SA2+TT) because of different intergranular carbide growth kinetics.

The SCC test was performed with a C-ring fabricated according to ASTM G38-01 at 315 °C in the static 40% NaOH solution at potential of 150 mV above the open circuit potential to understand the effect of the serrated grain boundary on SCC resistance. The 40% NaOH solution was purged with high purity nitrogen gas (99.9%) for 1 h to deaerate the solution in a 3.8L Ni autoclave. The reference electrode and counter electrode were external Ag/AgCl and platinum wire, respectively. Potential was applied with an EG&G 263 potentiostat. Crack length was measured at the cross section of a C-ring specimen with an optical microscope after the SCC test. The SCC rate was calculated by dividing the measured maximum crack length by the immersion time. The SCC test was also carried out in recirculating primary water at 360 °C with a slow strain rate of 10^{-7}/sec using a tensile specimen of 20% cold work to identify the relationship between grain boundary orientation with respect to the loading axis and its SCC resistance. Cold rolling was employed to produce 20% cold work of Alloy 600. The primary water contained 1200 ppm B, 2 ppm Li and 22 cc H_2/kg H_2O. The SCC test in primary water was strained up to 5%, and then the crack distribution in the tensile specimen surface was examined with a scanning electron microscope. For all SCC test, 3 specimens were used for each condition.

Table 1
Chemical composition of Alloy 600.

C	Cr	Ni	Fe	Si	Mn	S	Cu
0.04	15.4	75.1	8.0	0.1	0.3	<0.001	0.2

3. Results and discussion

3.1. Serrated grain boundary

Fig. 1(a) and (b) show the straight grain boundary and serrated grain boundary in Alloy 600, respectively. The white particles in the grain boundary are chromium carbide. Chromium carbides showed a closely spaced distribution in the straight boundary because heat treatment was performed at 710 °C for 15 h, whereas relatively coarse V shaped chromium carbide showed a widely spaced distribution in the serrated grain boundary because of slow cooling of 0.3 °C/min from the solution annealing temperature. These observations are consistent with the classical precipitation theory that nucleation rates are fast and growth rates are sluggish at low temperature which may result in semi continuous precipitation of carbides and vice versa. The average serration angle was about 45° for the specimen in this work, as shown in Fig. 2, where the serration angle φ is defined as the angle between the serrated boundary and a straight line connecting the peak of the serration boundary. A serrated grain boundary was reported in nickel base and cobalt base super alloys and in some ceramic materials [28–30]. A common feature of materials with a serrated grain boundary is that the precipitate and matrix have the same crystal structure and the lattice parameter of the precipitate is similar to or multiple times that of the matrix [28]. Several mechanisms have been proposed to explain serrated grain boundary formation. Larson [28] suggested that the serrated grain boundary formation is associated with the heterogeneous nucleation of γ′ at the grain boundaries, and the migration of grain boundary sections between the primary γ′ particles. Koul [34] proposed that the net strain energy difference between the matrix side and the boundary side of the particle matrix interface provided a driving force for the movement of primary γ′ particles in the direction of the boundary. On the other hand, Hong [30] suggested that the serrated grain boundary formation is related with asymmetric growth of precipitates.

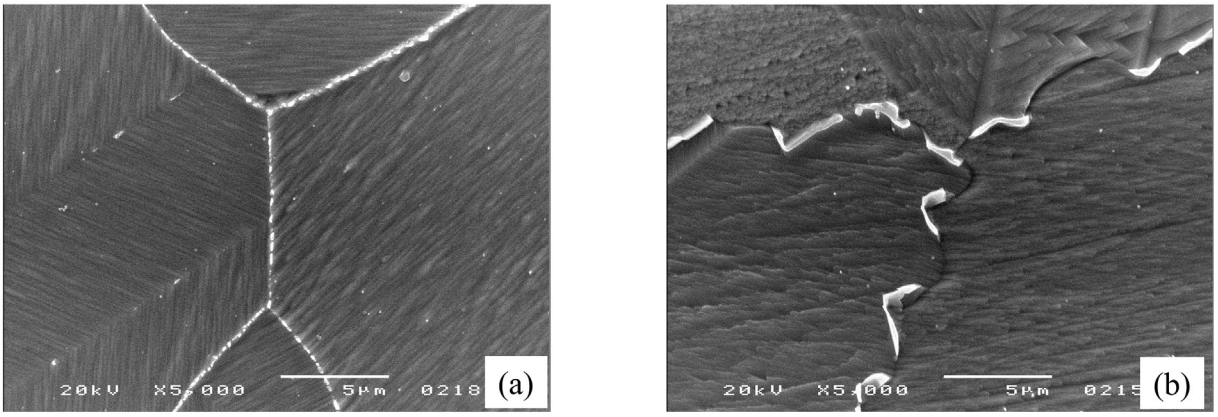

Fig. 1. Morphologies of straight grain boundary of SA2+TT (a) and serrated grain boundary of SA1+SERR (b).

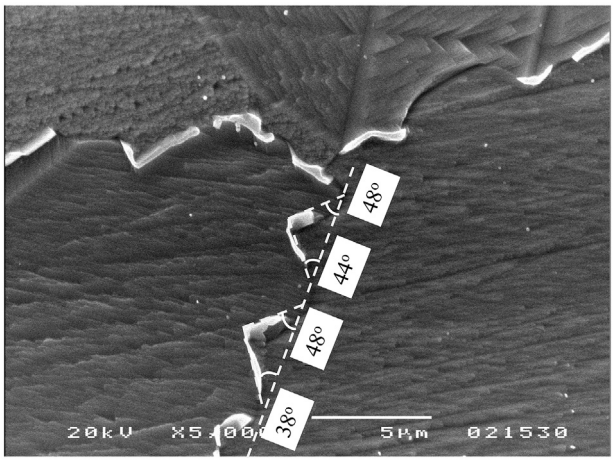

Fig. 2. Serration angle in serrated grain boundary of SA1+SERR.

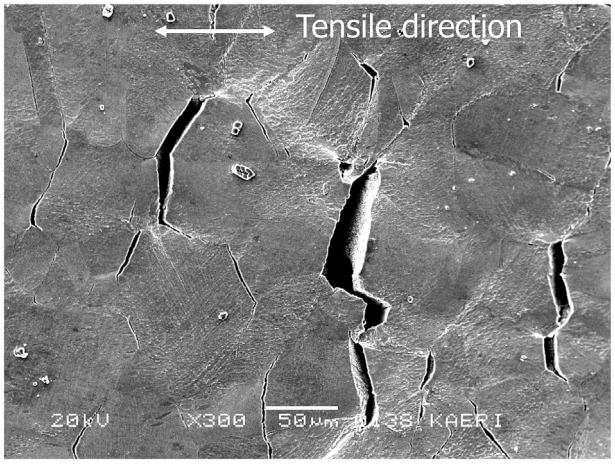

Fig. 3. Preferential stress corrosion cracking at grain boundary normal to tensile direction.

3.2. Tensile stress normal to grain boundary

A SCC test was performed in recirculating primary water at 360 °C with a slow strain rate of 10^{-7}/sec using a tensile specimen to identify the relationship between grain boundary orientation with respect to the loading axis and its SCC resistance. Fig. 3 shows that the SCC of cold worked Alloy 600 preferentially initiated and propagated at grain boundaries perpendicular to the loading direction in primary water of a pressurized water reactor. The phenomena were also observed in Alloy 690 and proton irradiated stainless steel [35,36]. In any kind of loading, the grain boundary area is a region where a series of mechanical constraints occur due to non-compatible slip. This results in damage at the grain boundary, such as grain boundary sliding induced by shear stress on the grain boundary and opening of the grain boundary induced by tensile stress normal to the grain boundary. Grain boundary sliding was observed experimentally [37]. In this case, the grain boundary can be seen as an additional "slip" plane, defined by the geometry instead of being defined by crystallography. Maximum shear stress occurs at 45° to the uniaxial loading direction. It appears that grain boundary slip is not a major factor influencing SCC in this work because SCC cracks were not observed at the grain boundary at 45° relative to the loading axis. Tensile stress normal to the grain boundary results in crack opening and a triaxial stress state ahead of a crack. The tensile stress normal to the grain boundary appears to be a major stress component in SCC because most small SCC cracks initiated at the grain boundary normal to tensile stress. The tensile stress may be due to applied load or residual stress. The residual stress can be induced by heat treatment, welding, machining, grinding, and cold work.

Resolved tensile stress perpendicular to the straight grain boundary σ_n is given by $F\sin\theta/l$, as shown in Fig. 4(a), where F is the load, l is the length and θ is the angle between the grain boundary and the loading axis. Even though stress is given by the load F divided by the area, in this work stress is defined as the load F divided by the grain boundary length based on the assumption that the grain boundary is vertical to the specimen surface. Resolved tensile stress perpendicular to the serrated grain boundary, σn1 is given by $F\sin(\theta-\varphi)\cos\varphi/l$ for the front part of the serrated boundary and σn2 $F\sin(\theta+\varphi)\cos\varphi/l$ for the rear part of the serrated boundary, as shown in Fig. 4(b).

Fig. 5 shows the tensile stress factor as a function of θ, where the stress factor is sinθ for the straight grain boundary and $\sin(\theta-\varphi)\cos\varphi$ for the front part of the serrated boundary and $\sin(\theta+\varphi)\cos\varphi$ for the rear part of the serrated boundary. When $\theta = 0°$, the stress factor on the straight boundary is always lower than that on the serrated grain boundary for any serration angle φ. When $\theta = 30°$, the stress factor on the straight boundary is higher than that on the serrated grain boundary for all serration angle φ at the front part of

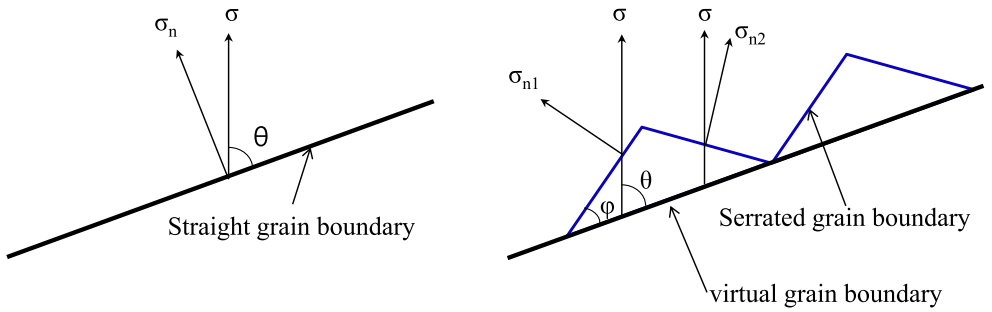

$\sigma_n = \sigma\sin\theta$

$\sigma_{n1} = \sigma\sin(\theta-\varphi)\cos\varphi$ at front part of serrated boundary

$\sigma_{n2} = \sigma\sin(\theta+\varphi)\cos\varphi$ at rear part of serrated boundary

(a) (b)

Fig. 4. Resolved tensile stresses normal to straight grain boundary (a) and serrated grain boundary (b).

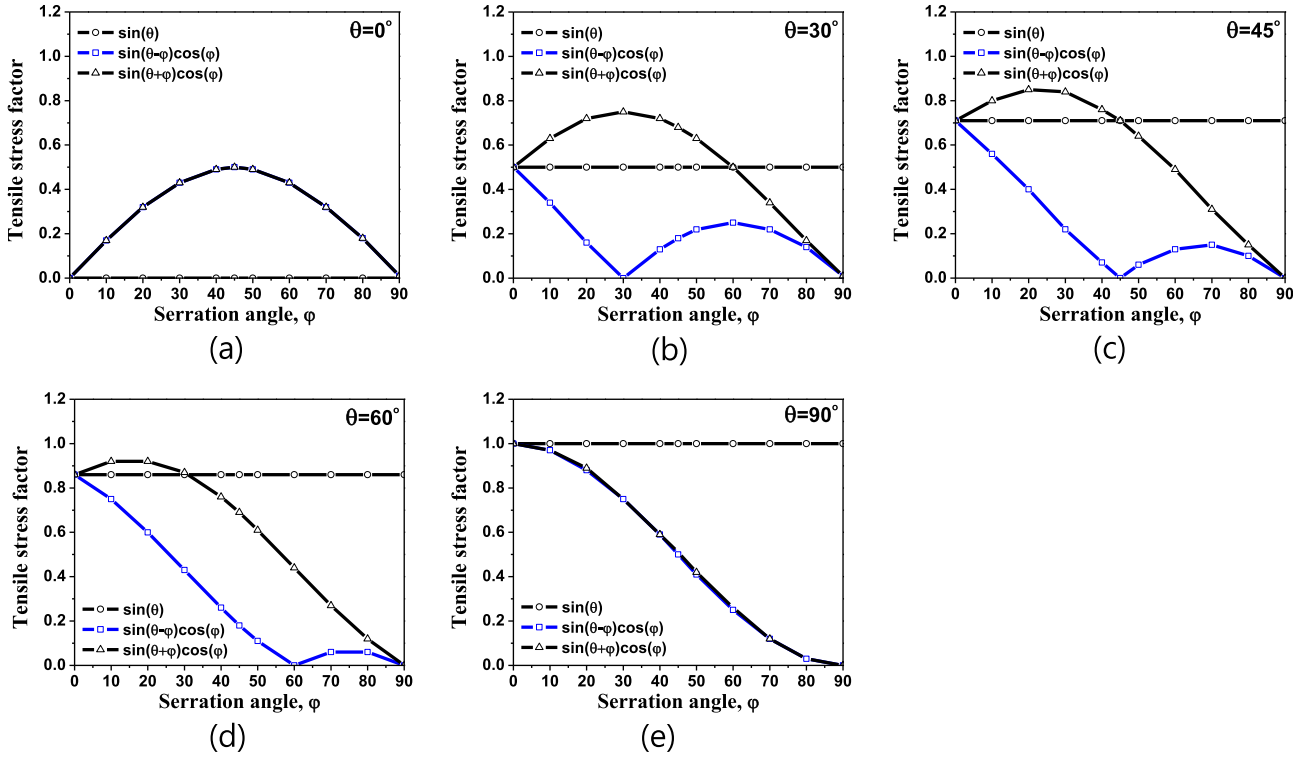

Fig. 5. Tensile stress factor versus serration angle (φ). Tensile stress factor of a straight grain boundary is sinθ (circle) and those of the front part and the rear part of the serrated grain boundary are sin (θ-φ)cosφ (rectangle) and sin (θ+φ)cos φ (triangle), respectively.

the serrated grain boundary and for a serration angle φ ranging from 60° to 90° at the rear part of the serrated grain boundary but lower for a serration angle φ ranging from 0° to 60° at the rear part of the serrated grain boundary. When θ = 60°, the stress factor on the straight boundary is only lower than that on the serrated grain boundary for a serration angle φ ranging from 0° to 30° at the rear part of the serrated grain boundary. When θ = 90°, the stress factor on the straight boundary is higher than that on the serrated grain boundary for all serration angles φ. This shows that the stress factor on the serrated grain boundary decreases with an increasing serration angle, which means that the SCC resistance can be improved by increasing the serration angle φ if the other microstructural features are the same.

Fig. 6 shows the stress factor for a typical serration angle of 45° observed in this work. Fig. 6(a) shows the stress factor for a straight grain boundary (circle), the front part of the serrated grain boundary (rectangle) and the rear part of the serrated grain boundary (triangle). Fig. 6(b) is a rearrangement of Fig. 6(a). It can be clearly deduced that the stress factor in the serrated grain boundary decreased by $1/\sqrt{2}$ (=cos 45°) for the serration angle of 45°.

3.3. Effect of serrated grain boundary on SCC in 40% NaOH solution

A SCC test was performed with a C-ring at 315 °C in a 40% NaOH solution at a potential of 150 mV above the open circuit potential to

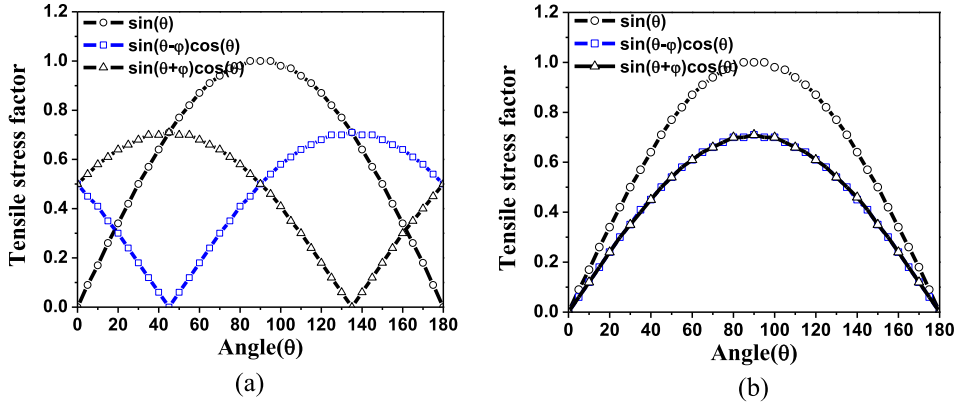

Fig. 6. Tensile stress factor versus the angle (θ) between loading axis and grain boundary for a serration angle of 45°. (a) Shows curves calculated directly from stress factors and (b) presents curves manipulated where stress factors of sin (θ-φ)cosφ for θ ranging from 0° to 45° moved and attached to 180° and stress factors of sin (θ+φ)cos φ for θ ranging from 135° to 180° moved and attached to 0°. Tensile stress factor of straight grain boundary is sinθ (circle) and that of the front part and the rear part of the serrated grain boundary is sin (θ-φ)cosφ (rectangle) and sin (θ+φ)cos φ (triangle).

understand the effect of the serrated grain boundary on SCC resistance. Cross-sectional area of C-ring specimen showing stress corrosion cracks is shown in Fig. 7. The SCC rate is shown in Fig. 8. SCC rates of the serrated grain boundary for SA1+SERR and SA1+SERR + TT specimens were about 34.7 and 83.3um/sec, respectively. Those of the straight grain boundary for SA2 and SA2+TT specimens were about 541.7 and 243.1 um/sec, respectively. SA2 specimens showed very high SCC rates because of the intergranular carbide-free microstructure [22]. The average intergranular carbide length and grain boundary coverage were 2.97 μm and 61.6% for the serrated grain boundary (SA1+SERR specimen) and 0.54 μm and 71.8% for the straight grain boundary (SA2+TT specimen). The intergranular carbide grain boundary coverage is defined as sum of intergranualr carbide length divided by grain boundary length. As SA1+SERR specimen is further heat treated at 710 °C for 15 hrs the average intergranular carbide length and grain boundary coverage is thought to be slightly decreased because of intergranualr carbide coarsening. It is generally accepted that SCC resistance of Alloy 600 increases with intergranualr carbide grain boundary coverage [22]. Even though the serrated grain boundary has lower intergranualr carbide grain boundary coverage than the straight boundary, it has higher SCC resistance because of grain boundary serration. The ratio of the SCC rate of the serrated grain boundary with SA1+SERR + TT to that of the straight grain boundary with SA2+TT is about 1/3. SA1+SERR + TT shows lower SCC resistance than SA1+SERR probably due to coarsening of the intergranualr carbide during thermal treatment. The stress effect on the SCC rate was reported to be proportional to σ^4 [38]. If the serration angle is 45°, the resolved normal tensile stress on the serrated grain boundary will be lower by a factor of $1/\sqrt{2}$ and then the SCC rate will be lower by a factor of 1/4 if the other microstructural features are the same. Many microstructural features such as grain size, bulk Cr content, and intergranular carbide density affect the SCC rate. It is best to identify the effect of the serrated grain boundary on SCC at the same microstructural features except

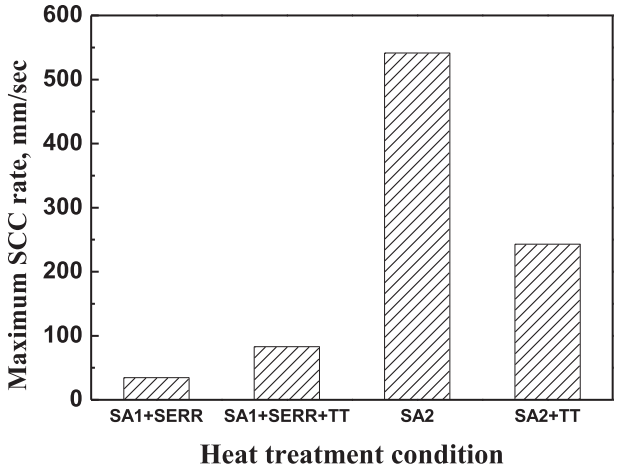

Fig. 8. SCC rate for serrated grain boundaries and straight grain boundaries.

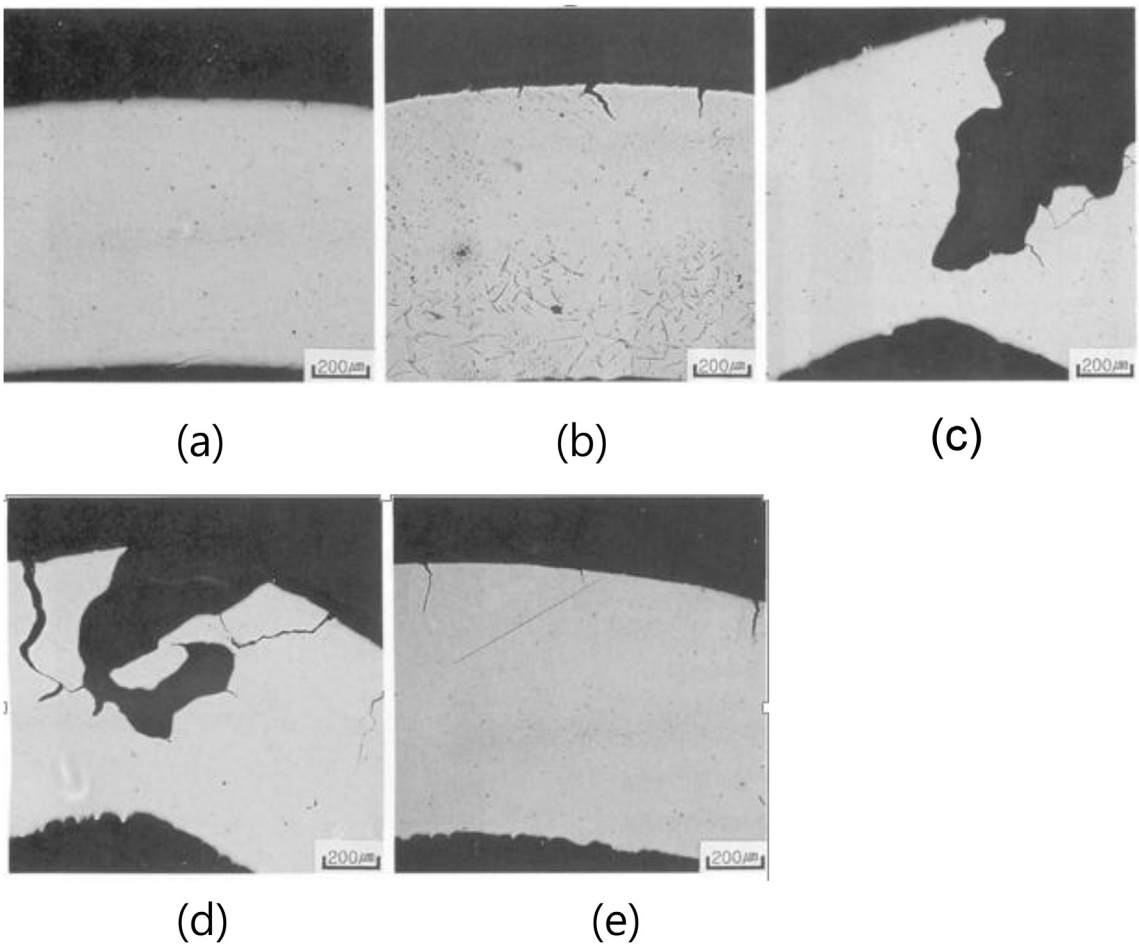

Fig. 7. Micrograph of cross-sectional area of C-ring specimen showing stress corrosion cracks. (a) SA + SERR, (b) SA + SERR + TT, (c) SA, (d) SA + SEN, (e) SA + TT.

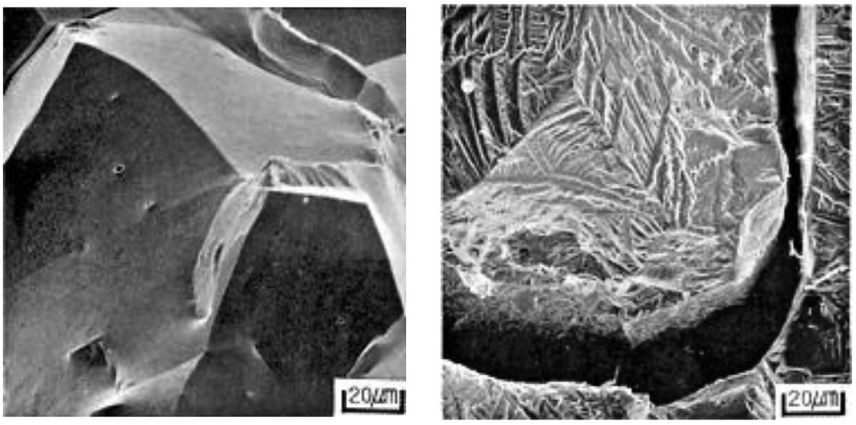

Fig. 9. SCC fracture surfaces of straight grain boundary of SA2+TT (a) and serrated grain boundary of SA1+SERR (b).

for the grain boundary configuration. Very similar grain sizes were obtained in this work for the serrated grain boundary and the straight grain boundary by changing the solution annealing temperature and time and the cooling rate. However, the morphologies of intergranular carbide were not the same for the serrated grain boundary and the straight grain boundary because the nucleation and growth temperature of intergranular carbide differ between these boundary types. Nucleation and growth of intergranular carbide occurs at higher temperature for the serrated grain boundary, and consequently the length of the intergranular carbide is longer than that of the straight grain boundaries. Almost continuous small intergranular carbide was observed in the straight grain boundaries because of the lower precipitation temperature. These differences in microstructural features in the serrated grain boundary and the straight grain boundary may lead to differences in the measured ratio and the calculated ratio of SCC rates. Because there are similarities for SCC in terms of microstructural features in a reducing environment of both primary water and caustic secondary water [39,40], high SCC resistance of a serrated grain boundary in a caustic solution could be applied to primary water.

The SCC fracture surfaces are shown in Fig. 9 for specimens with a straight grain boundary and a serrated grain boundary. The SCC fracture surfaces for the specimen with a straight grain boundary (Fig. 9(b)) shows a smooth fracture surface, which is consistent with intergranular fracture of the straight grain boundary. The SCC fracture surface of the specimen with a serrated grain boundary (Fig. 9(b)) shows a zigzag fracture surface, which is consistent with intergranular fracture of the serrated grain boundary.

4. Conclusion

The effect of a serrated grain boundary on stress corrosion cracking (SCC) of Alloy 600 was investigated in terms of improvement of SCC resistance. SCC cracks preferentially initiated and grew at the grain boundaries normal to the tensile loading axis. Resolved tensile stress normal to the grain boundaries was lower by a factor of $\cos\varphi$ in serrated grain boundaries compared to straight grain boundaries where φ is the serration angle. The specimen with serrated grain boundaries showed higher SCC resistance than that with straight grain boundaries. This appears to be caused by the serrated grain boundary having lower resolved tensile stress normal to the grain boundary.

Acknowledgements

This work was supported by a National Research Foundation of Korea grant funded by the Korean government (MSIP).

References

[1] P.E. Macdonald, V.N. Shah, L.W. Ward, P.G. Ellison, Steam Generator Tube Failures, NUREG/CR, 1966, pp. 78–114, 6365.
[2] P. Tran, PWR Steam Generator Replacement Survey Results, EPRI, 2005, 1011259.
[3] B. Grimmel, U.S. Plant Experience with Alloy 600 Cracking and Boric Acid Corrosion of Light-water Reactor Pressure Vessel Materials, NUREG, 2005, pp. 9–13, 1823.
[4] Y.S. Lim, H.P. Kim, S.S. Hwang, Microstructural characterization on intergranular stress corrosion cracking of alloy 600 in PWR primary water environment, J. Nucl. Mater. 440 (2013) 46–54.
[5] Y.S. Yi, S.H. Eom, H.P. Kim, J.S. Kim, Nickel boride (NiB) as an inhibitor for an IGSCC of alloy 600 and its applicability, J. Nucl. Mater. 347 (2005) 151–160.
[6] Y.S. Lim, S.S. Hwang, S.W. Kim, H.P. Kim, Primary water stress corrosion cracking behavior of an alloy 600/182 weld, Corros. Sci. 100 (2015) 12–22.
[7] S.S. Hwang, Y.S. Lim, S.W. Kim, D.J. Kim, H.P. Kim, Role of grain boundary carbides in cracking behavior of Ni base alloys, Nucl. Eng. Tech. 45 (2013) 73–79.
[8] S.S. Hwang, H.P. Kim, SCC analysis of alloy 600 tubes from a retired steam generator, J. Nucl. Mater. 440 (2013) 129–135.
[9] S.S. Hwang, H.P. Kim, D.H. Lee, U.C. Kim, J.S. Kim, The mode of stress corrosion cracking in Ni-base alloys in high temperature water containing lead, J. Nucl. Mater. 275 (1999) 28–36.
[10] S.S. Hwang, H.P. Kim, Y.S. Lim, J.S. Kim, L. Thomas, Transgranular SCC mechanism of thermally treated alloy 600 in alkaline water containing lead, Corros. Sci. 49 (2007) 3797–3811.
[11] S.W. Kim, H.P. Kim, Electrochemical noise analysis of PbSCC of Alloy 600 SG tube in caustic environments at high temperature, Corros. Sci. 51 (2009) 191–196.
[12] B.S. Rho, H.U. Hong, S.W. Nam, Analysis of the intergranular cavitation of Nb-a 286 alloy in high temperature low cycle fatigue using EBSD technique, Scr. Mater. 43 (2000) 167–173.
[13] M. McMurtrey, G. Was, L. Patrick, D. Farkas, Relationship between localized strain and irradiation assisted stress corrosion cracking in an austenitic alloy, Mater. Sci. Eng. A 528 (2011) 3730–3740.
[14] K. Fukuya, H. Nishioka, K. Fujii, T. Miura, T. Torimaru, An EBSD examination of SUS316 stainless steel irradiated to 73 dpa and deformed at 593 K, J. Nucl. Mater. 417 (2011) 958–962.
[15] E. West, G. Was, A model for the normal stress dependence of intergranular cracking of irradiated 316 L stainless steel in supercritical water, J. Nucl. Mater. 408 (2011) 142–152.
[16] E.A. West, M.D. McMurtrey, Z. Jiao, G.S. Was, Role of localized deformation in irradiation-assisted stress corrosion cracking initiation, Metall. Trans. A 43 (2012) 136–146.
[17] T. Watanabe, An approach to grain boundary design for strong and ductile polycrystals, Res. Mechanica 11 (1984) 47–84.
[18] G. Palumbo, P. King, P. Lichtenberger, K. Aust, U. Erb, Grain boundary design and control for intergranular stress-corrosion resistance, Scr. Metall. Mater. 25

(1991) 1775–1780.
[19] E.M. Lehockey, A.M. Brennenstuhl, I. Thompson, On the relationship between grain boundary connectivity, coincident site lattice boundaries, and intergranular stress corrosion cracking, Corros. Sci. 46 (2004) 2383–2404.
[20] V. Gertsman, S.M. Bruemmer, Study of grain boundary character along intergranular stress corrosion crack paths in austenitic alloys, Acta Mater. 49 (2001) 1589–1598.
[21] J. Gorman, PWR Reactor Vessel Alloy 600 Issues', Companion Guide to the ASME Boiler & Pressure Vessel Code : Criteria and Commentary on Select Aspects of the Boiler & Pressure Vessel and Piping Codes, ASME press, 2009 (chapter 44).
[22] J. Harris, V. Moroney, J. Gorman, Pressurized Water Reactor Generic Tube Degradation predictions-U.S. Recirculating Steam Generators with Alloy 600TT and Alloy 690TT, EPRI, July 2003, 1003589.
[23] S.I. Baik, M.J. Olszta, S.M. Bruemmer, D.N. Seidmana, Grain-boundary structure and segregation behavior in a nickel-base stainless alloy, Scr. Mater. 66 (2012) 809–812.
[24] H. Kawamura, H. Hirano, Role of grain boundary characteristics in caustic IGA/SCC resistance of thermally-treated Alloy 690 and shot-peened Alloy 800, in: Proc. 9th 11th International Symposium on Environmental Degradation of Materials in Nuclear Power System–Water Reactors, 1999, pp. 601–610.
[25] C. Shoemaker, in: Proc.: Workshop on Thermally Treated Alloy 690 Tubes for Nuclear Steam Generators (NP-4665S-sr), EPRI, Palo Alto, CA, 1986.
[26] S.S. Hwang, H.P. Kim, D.H. Lee, U.C. Kim, J.S. Kim, Corrosion behavior of Ni-based alloys in lead-contaminated water, in: Proc. Contributions of Materials Investigation to the Resolution of Problems Encountered in Pressurized Water Reactors, vol. 1, French Nuclear Energy Society, Societe Francaise d'Energie Nucleaire [SFEN], Fontevraud, France, 1998, pp. 403–415.
[27] T. Sakai, T. Senjuh, K. Aoki, T. Shigemitsu, Y. Kishi, Lead-Induced stress corrosion cracking of Alloy 600 and 690 in high-temperature water, in: Proc. 5th International Symposium on Environmental Degradation of Materials in Nuclear Power System–Water Reactors, 1991, pp. 764–772.
[28] J.M. Larson, S. Floreen, Metallurgical factors affecting the crack growth resistance of a superalloy, Metall. Trans. A 8 (1977) 51–55.
[29] H. Loyer Danflou, M. Marty, A. Walder, in: S.D. Antolovich, R.W. Stusrud, R.A. MacKay, D.L. Anton, T. Khan, R.D. Kissinger, D.L. Klarstrom (Eds.), Superalloys, the Minerals, Metals, and Materials Society, Warrendale, PA, 1992, pp. 63–72.
[30] H.U. Hong, I.S. Kim, B.G. Choi, M.Y. Kim, C.Y. Jo, The effect of grain boundary serration on creep resistance in a wrought nickel-based superalloy, Mat. Sci. Eng. A 517 (2009) 125–131.
[31] G.H. Bishop, W.H. Hartt, G.A. Bruggeman, Grain boundary faceting of (1010) tilt boundaries in zinc, Acta Metall. 19 (1971) 37–46.
[32] T.E. Hsieh, R.W. Balluffi, Observations of roughening/de-faceting phase transitions in grain boundaries, Acta Metall. Mater. 37 (1989) 2133–2139.
[33] K.J. Kim, H.U. Hong, S.W. Nam, A study on the mechanism of serrated grain boundary formation in an austenitic stainless steel, Mater. Chem. Phys. 126 (2011) 480–483.
[34] A.K. Koul, G.H. Gessinger, On the mechanism of serrated grain boundary formation xn ni-based superalloys, Acta Metall. 31 (1983) 1061–1069.
[35] A. Stratulat, J.A. Duff, T.J. Marrow, Grain boundary structure and intergranular stress corrosion crackinitiation in high temperature water of a thermally sensitized austenitic stainless steel, observed in situ, Corros. Sci. 85 (2014) 428–435.
[36] E. West, G. Was, A model for the normal stress dependence of intergranular cracking of irradiated 316 L stainless steel in supercritical water, J. Nucl. Mater. 408 (2011) 142–152.
[37] B. Alexandreanu, Grain Boundary Deformation-induced Intergranular Stress Corrosion Cracking of Ni–16Cr–9Fe in 360oC Water, Ph. D. Thesis, University of Michigan, Ann Arbor, MI, 2002.
[38] R. Bandy, D. van Rooyen, Tests with Inconel 600 to Obtain Quantitative Stress Corrosion Cracking Data for Evaluating Service Performance, BNL-NUREG-31814, U.S. Nuclear Regulatory Commission, Washington, DC, 1983.
[39] G.P. Airey, The effect of carbon content and thermal treatment on the SCC behavior of Inconel Alloy 600 steam generator tubing, Corrosion 35 (1979) 129–136.
[40] J.R. Crum, Effect of composition and heat treatment on stress corrosion cracking of Alloy 600 steam generator tubes in sodium hydroxide, Corrosion 38 (1982) 40–45.